Different approaches to analyze the dipolar interaction effects on diluted and concentrated granular...

Article *in* Journal of Magnetism and Magnetic Materials · April 2017

DOI: 10.1016/j.jmmm.2016.12.019

CITATIONS
0

READS
116

13 authors, including:

Oscar Moscoso Londoño
University of Campinas
18 PUBLICATIONS **41** CITATIONS
SEE PROFILE

Marcela B. Fernández van Raap
National University of La Plata
67 PUBLICATIONS **364** CITATIONS
SEE PROFILE

Marcelo Knobel
University of Campinas
526 PUBLICATIONS **6,221** CITATIONS
SEE PROFILE

Leandro M. Socolovsky
University of Buenos Aires
74 PUBLICATIONS **710** CITATIONS
SEE PROFILE

Journal of Magnetism and Magnetic Materials 428 (2017) 105–118

Contents lists available at ScienceDirect

Journal of Magnetism and Magnetic Materials

journal homepage: www.elsevier.com/locate/jmmm

Different approaches to analyze the dipolar interaction effects on diluted and concentrated granular superparamagnetic systems

O. Moscoso-Londoño[a,*], P. Tancredi[b], D. Muraca[a,c], P. Mendoza Zélis[d], D. Coral[d], M.B. Fernández van Raap[d], U. Wolff[e], V. Neu[e], C. Damm[e], C.L.P. de Oliveira[f], K.R. Pirota[a], M. Knobel[a,g], L.M. Socolovsky[b,*]

[a] Instituto de Física 'Gleb Wataghin', Universidade Estadual de Campinas (UNICAMP), CEP13083-859 Campinas, São Paulo, Brazil
[b] Laboratorio de Sólidos Amorfos, INTECIN, Facultad de Ingeniería, Universidad de Buenos Aires (UBA), CONICET, C1063ACV Buenos Aires, Argentina
[c] Centro de Ciencias Naturais e Humanas, Universidade Federal do ABC (UFABC), Av. Dos Estados, 5001, Santo André, SP, Brazil
[d] Instituto de Física, Universidad Nacional de La Plata (UNLP), CONICET, CC.67, 1900 La Plata, Buenos Aires, Argentina
[e] IFW Dresden, Leibniz Institute for Solid State and Materials Research, Dresden, Helmholtzstrasse 20, 01069 Dresden, Germany
[f] Instituto de Física, Universidade de São Paulo, São Paulo 05314970, Brasil
[g] Laboratório Nacional de Nanotecnologia (LNNano/CNPEM), Rua Giuseppe Máximo Scolfaro 10000, 13083-100, Campinas, São Paulo, Brazil

ARTICLE INFO

Keywords:
Magnetic nanoparticles
Dipolar interactions
Interacting superparamagnetic model
Small-angle X-ray scattering
Cluster formation

ABSTRACT

Controlled magnetic granular materials with different concentrations of magnetite nanoparticles immersed in a non-conducting polymer matrix were synthesized and, their macroscopic magnetic observables analyzed in order to advance towards a better understanding of the magnetic dipolar interactions and its effects on the obtained magnetic parameters. First, by means of X-ray diffraction, transmission electron microscopy, small angle X-ray scattering and X-ray absorption fine structure an accurate study of the structural properties was carried out. Then, the magnetic properties were analyzed by means of different models, including those that consider the magnetic interactions through long-range dipolar forces as: the Interacting Superparamagnetic Model (ISP) and the Vogel-Fulcher law (V-F). In systems with larger nanoparticle concentrations, magnetic results clearly indicate that the role played by the dipolar interactions affects the magnetic properties, giving rise to obtaining magnetic and structural parameters without physical meaning. Magnetic parameters as the effective anisotropic constant, magnetic moment relaxation time and mean blocking temperature, extracted from the application of the ISP model and V-F Law, were used to simulate the zero-field-cooling (ZFC) and field-cooling curves (FC). A comparative analysis of the simulated, fitted and experimental ZFC/FC curves suggests that the current models depict indeed our dilute granular systems. Notwithstanding, for concentrated samples, the ISP model infers that clustered nanoparticles are being interpreted as single entities of larger magnetic moment and volume, effect that is apparently related to a collective and complex magnetic moment dynamics within the cluster.

1. Introduction

The study of nanostructured systems composed of magnetic nanoparticles dispersed in organic polymeric matrices has attracted much interest in the last years, owing to the richness of the involved physics behind their fundamental properties, and also due to potential applications in technological and biomedical areas [1,2]. These types of granular magnetic nanocomposites are a new kind of stimuli-responsive smart materials, as they can change their volume, viscosity, internal stress or structure in response to variations of an external magnetic field [3,4]. Owing to the synergy between the magnetic nanoparticles and the non-conducting polymer matrix, these materials play an important role in the development of new devices of fundamental interest in biomedical and pharmaceutical fields such as biosensors, artificial muscles, and drug delivery systems, among others [5–8].

The assemblage between the magnetic nanoparticles and a non-magnetic polymer matrix can be achieved by diverse techniques, including chemical crosslinking, photo-polymerization, electron irradiation or freezing–thawing [9–12]. Among the polymer raw materials employed so far, highly-biocompatible and inexpensive polyvinyl alcohol (PVA) is one of the most popular polymers for stimuli-

* Corresponding authors.
E-mail addresses: omoscoso@ifi.unicamp.br (O. Moscoso-Londoño), lsocolovsky@fi.uba.ar (L.M. Socolovsky).

http://dx.doi.org/10.1016/j.jmmm.2016.12.019
Received 10 August 2016; Received in revised form 9 December 2016; Accepted 9 December 2016
Available online 16 December 2016
0304-8853/

responsive magnetic materials elaboration. The composite PVA – hydrophilic iron oxide nanoparticles (IONPs) has been extensively studied, mainly in investigations of nanoparticle incorporation, effect of nanoparticle coating on the matrix distribution, drug release or protein absorption behavior [13–15].

In addition, nanocomposites with controlled concentration of magnetic solute are very useful to experimentally study some fundamental aspects of magnetism at the nanoscale [16,17]. The advantages of employing these materials compared to other granular systems, such as the ones obtained by melt-spinning or co-deposition, rely on the straightforward structural characterization and narrower size distributions of the magnetic entities [18,19]. The preparation of polymer magnetic nanocomposites is highly controllable, from the synthesis of the magnetic active component to its well-dispersion and control of the spatial distribution within the hosting matrix. These features allow overcoming the usual drawbacks like particle size and shape, or atoms forming channels into the same structure [20], making these systems suitable candidates to perform fundamental magnetic studies.

Specifically speaking of those systems in which the hosting matrices are loaded with single-domain magnetic nanoparticles, to better understand the macroscopic magnetic response of these nanocomposites it is fundamental to consider the role played by magnetic interactions among the nanoparticles. Typically, interacting magnetic systems display a different behavior when compared to the non-interacting ones [21–24]. For example, experimental evidence suggests that the long-range magnetic dipole-dipole interactions affect several magnetic properties, such as the blocking temperature, energy barrier or the heating efficiency during the application of AC magnetic fields [24–26], among others. Despite the development of new models and theories to recreate real systems composed by magnetic nanoparticles, it is rather complicated to separate the role of dipolar interactions from other features, such as clustering effects, surface effects, shape and size distributions, among others. Some approaches have been proposed to explain the experimental data departing from the expected behavior, such as changes in the energy barriers in isolated particles, or progressive and dependent blocking of particles induced by collective phenomena [18,27–30].

In this work, we study the effect of dipolar interactions on different magnetic properties of nanoparticles diluted and clustering in polymeric matrices. The nanoparticles and polymer were extensively studied to fully characterize the nanostructure, and discard other possible effects besides magnetic interactions among nanoparticles. To this end, two diluted and two concentrated samples (PVA-IONPs) were prepared. By incorporating different amounts IONPs a direct correlation between the spatial distribution of the magnetic entities and the strengthening of magnetic dipolar interactions was reached. The results indicate that the strengthening of the dipolar nanoparticle interaction promotes a progressive shift of the magnetic parameter values towards non-realistic ones. To tackle this challenge we applied an advanced model for magnetic dipolar interactions (ISP) formulated by Allia et al. [29] as well as the Vogel-Fulcher law (V-F). From the ISP and V-F outcomes we have simulate the zero-field-cooling (ZFC) and field-cooling (FC) curves, concluding that for diluted systems (weakly interacting), these models are reliable. However, for the two most concentrated samples (highly interacting), we detected that the ISP model describes clusters of nanoparticles as if they were single and larger magnetic entities, that phenomena can be product of a complex magnetic behavior that could emerge from two main sources; (i) interaction among the clustered nanoparticles and (ii) between clusters. Such evidence allows us to extract information, as for example the cluster magnetic volume.

2. Experimental details

All the reagents used in this work were analytical grade and used without further purification. Iron (III) chloride hexahydrate ($FeCl_3 \cdot 6H_2O$, 97%, Tetrahedron), iron (II) sulphate heptahydrate ($FeSO_4 \cdot 7H_2O$, ≥99%, Sigma-Aldrich), sodium hydroxide (NaOH, 99%, Anedra), polyvinyl alcohol (PVA, fully hydrolyzed, Sigma-Aldrich), citric acid ($C_6H_8O_7$, > 99% Cicarelli). Deionized water was used in all syntheses.

2.1. Synthesis of citric acid-coated Fe_3O_4 nanoparticles

Magnetic iron oxide nanoparticles (IONPs) were prepared by the co-precipitation method [31]. Briefly, 7.5 g of NaOH were dissolved in 125 mL of H_2O. Then, a mixture of 18 mmol of $FeCl_3 \cdot 6H_2O$ and 9 mmol of $FeSO_4 \cdot 7H_2O$ dissolved in 25 mL of H_2O was added dropwise to the NaOH solution under Ar atmosphere and vigorous stirring. After 30 min, 8.3 g of citric acid was added to produce hydrophilic-carboxyl coated IONPs. The temperature was then raised to 80 °C and maintained for 30 min. Citric-coated IONPs were magnetically decanted and suspended in H_2O until a stable suspension with pH=7 was obtained. This ferrofluid was named S_{FF}. For some structural characterizations, such as XRD or FTIR, the stable dispersions of citric coated-IONPs were magnetically decanted after adding acetone and dried in vacuum in order to obtain a powder sample. Such sample was labeled as S_{PO}.

2.2. Synthesis of magnetic gels: citric acid-coated Fe_3O_4 in PVA matrixes

Magnetic polymer nanocomposites were prepared by crosslinking PVA with different dilutions of S_{FF} in order to achieve dispersion of different IONPs concentrations. PVA solutions were first prepared by mixing 10 g of polymer and 100 mL of H_2O at 85 °C under continuous stirring for 4 h. After this process, 5 mL of four different dilutions of S_{FF} were mixed with 15 mL of the PVA solutions to produce the samples with 0.5 wt%, 3 wt%, 15 wt% and 30 wt% of citric coated-IONPs, with respect to the total content. These dispersions were poured into molds, frozen for 3 h (−18 °C) and allowed to thaw at room temperature (25 °C) for the same time. This freezing–thawing process was repeated 3 times in order in order to trigger the cross-linkings. The so obtained samples are labeled as $S_{0.5\%}$, $S_{3\%}$, $S_{15\%}$ and $S_{30\%}$ for magnetic composites loaded with 0.5 wt%, 3 wt%, 15 wt% and 30 wt% of citric-coated IONPs, respectively.

2.3. Characterization

X-ray diffraction (XRD) patterns were obtained by standard Rigaku diffractometer with Cu-Kα radiation (λ=1.5406 Å). Rietveld analysis was performed using the package GSAS [32] with EXPGUI as graphical interface [33]. Transmission electron microscopy (TEM) images were collected with a FEI-Tecnai™ microscope. Fourier transform infrared (FTIR) spectra were carried out at room temperature in the range of 400–4000 cm^{-1} employing a Shimadzu infrared spectrometer model IR-Prestige 21, using KBr disks method. X-ray absorption fine structure (XAFS) spectroscopy spectra at the Fe K-edge (7.112 keV) were collected at the Brazilian Synchrotron Light Laboratory (LNLS, Campinas, Brazil) at room temperature. XANES and EXAFS data for $S_{3\%}$, $S_{15\%}$ and $S_{30\%}$ samples were recorded in transmission mode. Owing to the low Fe concentration in sample $S_{0.5\%}$ the XANES and EXAFS data were obtained in the fluorescence mode with the sample positioned 45° with respect to the beam. Small angle X-ray scattering (SAXS) experiments were performed in a NANOSTAR™ camera (Bruker), equipped with a Xenocs Genix3D microfocus X-ray source (λ=1.541 Å). The beam collimation was performed with two sets of scatterless slits, also provided by Xenocs. The sample to detector distance of 670 mm was used to cover a scattering range (q) from 0.09 up to 2.8 nm^{-1}. The scattering intensity was measured as function of $q = 4\pi \sin(\frac{\theta}{\lambda})$; where 2θ is the scattering angle. SAXS data were recorded in vacuum and at room temperature using exposition times

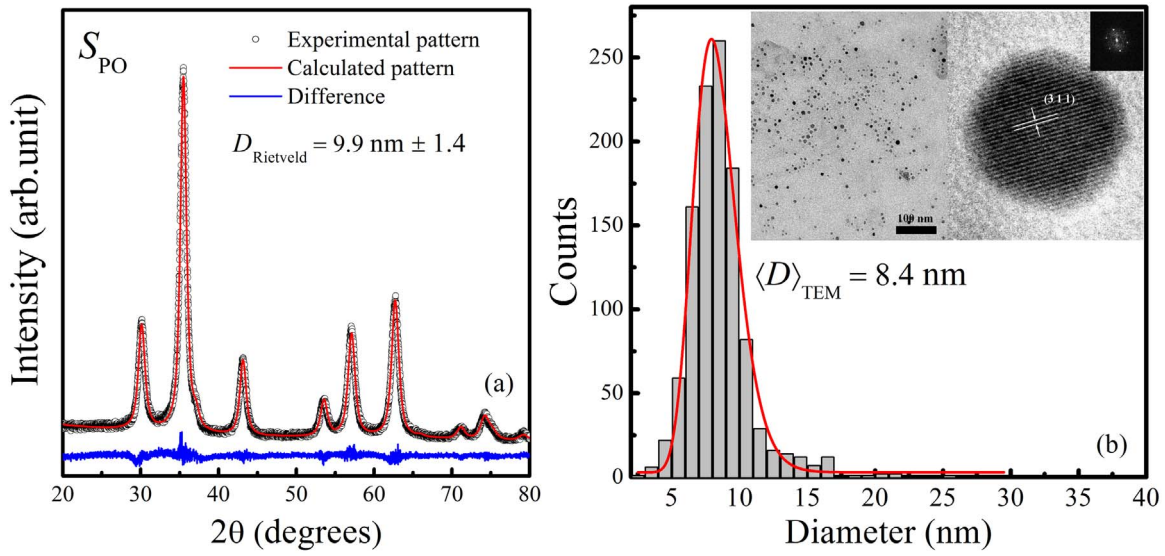

Fig. 1. (a) X-Ray diffraction pattern of citric acid coated iron oxide nanoparticles (symbols). Rietveld refinement results are shown as a continuous red line. (b) Histogram (bars) and lognormal fit (line) of nanoparticle size distribution derived from TEM analysis. *Inset*: TEM images of the iron oxide nanoparticles with two different magnification. The Fourier transform is also shown. (For interpretation of the references to color in this figure legend, the reader is referred to the web version of this article.)

of 900 s, data treatment was performed using the SASfit package [34].

DC magnetic properties (ZFC-FC and M-H curves) of the nanocomposites were studied on a Quantum Design-PPMS with a vibrating sample magnetometer head (VSM). AC magnetic susceptibility measurements were performed by a Quantum Design-PPMS magnetometer in AC-mode transport head.

3. Structural characterization results

3.1. Structural and morphological characterization of citric acid coated-Fe_3O_4 nanoparticles

Size and crystallite structure of the as synthesized sample (S_{PO}) were evaluated by means of X-ray diffraction technique. As can be seen in Fig. 1(a), the obtained diffractogram of sample S_{PO} matches well with the Fe_3O_4 and/or γ-Fe_2O_3 crystalline pattern and confirms the formation of a pure fcc spinel-inverse iron oxide phase. The nanocrystallite size, calculated by Rietveld analyses (Fig. 1, red line), is 9.9 nm ± 1.4.

To confirm the disperse nature of the initial colloidal suspension (S_{FF}), as well as to know the nanoparticles shape and, to determine the nanoparticle size distribution were conducted experiments of transmission electron microscopy (TEM). According to the obtained images, the sample S_{FF} is composed of non-aggregated nanoparticles, each one with a nearly spherical shape. From it, the histogram (Fig. 1(b)) was built analyzing more than one thousand nanoparticles from several TEM images, which were properly fitted with a lognormal function. A mean diameter of 8.4 nm with narrow size distribution (σ=0.2) was determined. The measured interplanar distances (inset in Fig. 1(b)) are in good agreement with the lattice spacings of magnetite or maghemite crystals [35]. Moreover, from TEM images one can to infer that the citric acid capping (whose attachment was confirmed by FTIR analysis, see Fig. 1.SI) acts in order to avoid excessive agglomeration during the IONPs formation and, yields a stable ferrofluid with well-dispersed magnetic nanoparticles. Then, taking advantage this fact as well as that the citric acid carboxylate groups can interact with hydroxyl-rich PVA by ion-dipole forces, we can guarantee a fine particle dispersion within the PVA matrices, avoiding the nanoparticle percolation and ensuring a homogeneous distribution of these over the whole PVA volume. However, the formation of aggregates of nanometric size would be limited by the NPs concentration, as will be discussed later.

3.2. Examination of the Fe oxidation state. Fe-K-XAFS analysis

It is widely known that the magnetic observables of systems composed by iron oxide nanoparticles are determined by a large number of parameters as the average particle size, size distribution, shape, surface/volume ratio, Fe oxidation state and so on. Most of these parameters can be tuned in the synthesis procedure [36]. However, and due to the fact that the magnetite nanoparticles (Fe_3O_4) can easily transform into maghemite nanoparticles (γ-Fe_2O_3), even in environmental settings, the control of the oxidation state is required in order to explain the magnetic properties.

As the XRD analysis does not provide sufficiently accurate information to distinguish between structurally similar chemical Fe-mineral species such as magnetite, non-stoichiometric magnetite or maghemite, measures of X-Ray Absorption Spectroscopy was carried out to complement XRD results and to determine more accurately the oxidation states of the Fe. Then, exploiting the fact that this technique is sensitive to the local environment of absorbing atoms, we decided to analyze the local structure of the average Fe atoms by examining the Fe K-edge spectra.

According to the XANES patterns (Fig. 2(a)), the increasing in the nanoparticle concentration does not affect both the pre-edge region features neither the absorption edge position (7.126 keV). For all samples, the observed features are compatibles with a Fe^{3+} and Fe^{2+} mixture [37–40] and matches well with literature reports for non-stoichiometric magnetite phase [16]. The EXFAS region and the Fourier Transforms (FT) for the set of studied samples are showed in Fig. 2(b-e) and (f-i), respectively. All EXAFS profiles (obtained by conventional treatment) exhibit a characteristic signal formed by the contribution of the first and second oxygen neighbor as well as Fe^{2+} and Fe^{3+} ions. FT amplitudes (Fig. 2(f-i)) show a first broad peak between 0.9–2.1 Å, on the positions of the first and second Fe-O neighbors. The second peak exhibits two maxima at 2.6 Å and 3.0 Å, respectively, which are associated to Fe-Fe sub-shells. Comparing the both EXFAS and FT profiles, for all samples no significant changes were observed. It is evidence that the internal structure of the nanoparticles is not altered by the concentration of these. In this sense, as the bonding geometry around Fe remains unaltered in all samples, we can be sure that effects associated with percolated systems, as direct or indirect exchange interaction among surface Fe ions, does not have place in the synthesized samples. This point will allow us to relate the modifications in the magnetic response only with the

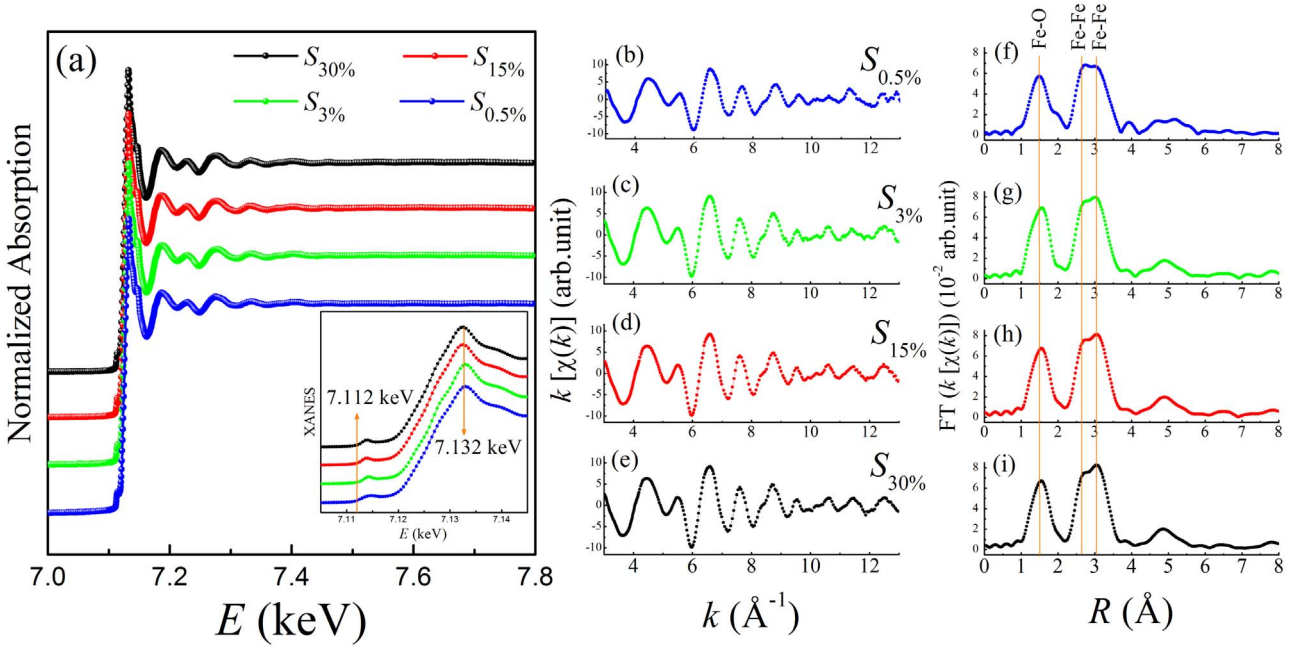

Fig. 2. (a) Comparison of the experimental Fe K-edge XAFS spectra for a series of IONPs-PVA prepared at nanoparticle concentrations of 0.5%, 3%, 15% and 30%. *Inset*: a detailed comparison of the experimental Fe K-edge XANES spectra for same samples. (b–e) EXAFS spectra and (f–i) Fourier transforms obtained for samples $S_{0.5\%}$, $S_{3\%}$, $S_{15\%}$ and $S_{30\%}$.

variation of the magnetic dipolar interactions.

Structural organization of the IONPs inside of the PVA matrSmall-angle X-ray scattering (SAXS) was employed to identify and quantify NPs agglomeration within the PVA matrix. Thus, the experimental SAXS data were analyzed using the unified exponential/power-law postulated by Beaucage and based on hierarchical structures [41]. Briefly, Porod and Guinier regimes are combined into a single equation to describe the scattering of any morphology of complex systems containing multiple levels of related structural features [41,42]. In our case, this law was applied to follow primary particle aggregation as their concentration rises into the PVA matrices. Then, the Beaucage expression for two scaling regimes used to describe the structure of primary nanoparticles and aggregates is given by:

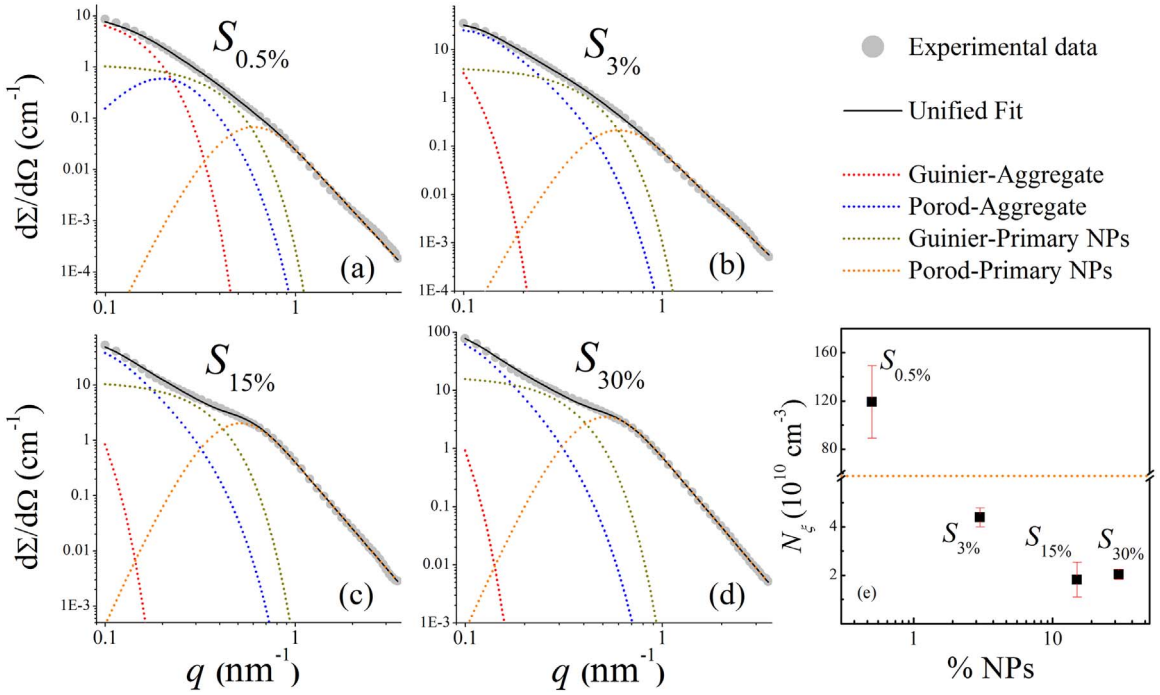

Fig. 3. (a-d) SAXS curves of the magnetic composites. The experimental data was fitted with SASFit package following the extended Beaucage expression described in the text. Contribution of the Guinier and Porod pre-factors G, B and G_{PP}, B_{PP} are presented as dotted lines. (e) Number density of magnetic aggregates (N_ξ) as a function of nanoparticle concentration.

$$\frac{d\Sigma}{d\Omega}(q) = G\exp\left[\frac{-q^2\xi^2}{12}\right] + B\exp\left[\frac{-q^2D_{PP}^2}{12}\right]\left(\frac{erf\left(\frac{q\xi}{2\sqrt{6}}\right)^3}{q}\right)^{d_F} + G_{PP}\exp\left[\frac{-q^2D_{PP}^2}{12}\right] + B_{PP}\left(\frac{erf\left(\frac{qD_{PP}}{2\sqrt{6}}\right)^3}{q}\right)^P \quad (1)$$

where the Guinier and Porod pre-factors of the aggregates are given by $G = N_\xi \Delta\eta^2 (\frac{4\pi}{3})^2 (\frac{\xi}{2})^6$ and $B = 2\pi N_{PP}\Delta\eta^2 S$, respectively. Being N_ξ the magnetic aggregates number density, N_{PP} the number of small subunits within each aggregate, $\Delta\eta$ the scattering length density difference between IONPs and the surrounding PVA matrix ($\Delta\eta$=3.06×10^{11} cm^{-2}), S the specific surface. G_{PP} and B_{PP} are the mentioned pre-factors for primary particles. *erf* is the error function, ξ and D_{PP} are the diameters of the aggregates and primary particles, respectively. The latter is related to the respective radii of gyration. d_F is the fractal dimension of the aggregates and, P is the Porod exponent.

Fig. 3 shows *log-log* plot of experimental SAXS data (symbols) taken on a specimen of every S sample. The SAXS patterns are distinctive of systems composed by polydisperse particles with two hierarchical levels, corresponding to aggregates and primary nanoparticles. For all of the SAXS patterns, in the low q region, the differential cross section, $\partial\Sigma(q)/\partial\Omega$, deviates from the typical Guinier behavior for individual particles, indicating that IONPs aggregation has occurred [43]. The scattering patterns of samples $S_{0.5\%}$ and $S_{3\%}$ (Fig. 3(a) and (b)) display a smooth decreasing q-behavior, while in the samples with highest nanoparticle concentration ($S_{15\%}$ and $S_{30\%}$) a knee appears at q≈0.5 nm^{-1}. A shift in this knee is generally attributed to changes in size of the scattering objects. However, in our case the same batch of nanoparticles were used to prepare each granular composite, whereby the shift in such knee-like decay could be attributed to stronger scattering interference between the neighboring iron oxide nanoparticles in samples $S_{15\%}$ and $S_{30\%}$, consistently with the establishment of a more compact architecture and large amount of magnetic solute. In the high q region, the scattered intensity decays with a q^{-4} power law. This behavior is characteristic of Porod scattering from smooth and sharp interfaces among iron oxide NPs and the polymer matrix [42,44].

Taking into account the primary nanoparticle aggregation and following their behavior as the nanoparticle concentration increases, SAXS was analyzed through the extended Beaucage expression described above. For fitting procedure, the single nanoparticle diameter was fixed at 8.4 nm (according to the TEM information). As can be seen in Fig. 3(a-d) the scattering data of all S magnetic composites were well described by the unified fit (Eq. (1)). The Guinier and Porod component curves of aggregates and primary nanoparticles are also shown the figure (dotted lines). Fitted d_F values were 2.47, 2.76, 2.81 and 2.99 for samples $S_{0.5\%}$, $S_{3\%}$, $S_{15\%}$ and $S_{30\%}$, respectively. These fractal dimension d_F values are indicating that the in all samples the aggregates has a spherical shape [45], which are composed by primary nanoparticles. The shift towards higher values indicates that the aggregates are more compact as the IONPs concentration fraction increases. The aggregate fractal dimension evolution was also studied by means of a fractal aggregate model (see in Supplementary information, section I-B), in which the d_F increase was confirmed. Fitted parameters are summarized in Table 1. The obtained aggregate size values (ξ) were 27 nm, 61 nm, 73 nm and 75 nm for $S_{0.5\%}$, $S_{3\%}$, $S_{15\%}$ and $S_{30\%}$, respectively. These ξ values, as well as their evolution with the IONPs concentration, are within the expected range taking into consideration previous reports based on similar systems [13,42,44,46,47].

To determine the density of magnetic aggregates (N_ξ) within the magnetic composites, the Guinier and Porod expressions (for aggregate structural level) were combined to obtain a functional ratio between the obtained SAXS parameters and N_ξ, being this:

Table 1.
SAXS Parameters ξ, d_F and N_ξ (defined in the text) obtained from the curve fitting using to Eq. (1).

Sample	ξ (nm)	d_F	N_ξ (10^{10} cm^{-3})
$S_{0.5\%}$	27	2.47	119 (30)
$S_{3\%}$	61	2.76	4.4 (0.4)
$S_{15\%}$	73	2.81	1.8 (0.7)
$S_{30\%}$	75	2.99	2.1 (0.2)

$$N_\xi = \frac{G}{\Delta\eta^2(\frac{4\pi}{3})^2(\frac{\xi}{2})^6} \quad (2)$$

Calculated N_ξ values are listed Table 1. and its evolution with the nanoparticle concentration is displayed in Fig. 3(e). The result indicates that in sample $S_{0.5\%}$ coexist more aggregates per unit volume (~10^{12} cm^{-3}) in comparison with other three samples (~10^{10} cm^{-3}). Then, as this sample present less compact aggregates of smaller size (in comparison to the others samples), it is possible to infer that in sample $S_{0.5\%}$ the special nanoparticle distribution it would not be limited by a concentration of 0.5 wt% and, the aggregate formation is just a consequence of the magnetic nature of the iron oxide nanoparticles.

In summary, our structural characterization contributed with useful information, proving that the Fe atomic environment and crystal structure remains unaltered in all synthesized samples. From SAXS analysis was confirmed the aggregate formation. Explicitly, three important features related to the nanoparticle architecture within the PVA matrices were determined: (*i*) the aggregate size, (*ii*) a qualitative idea of the aggregate compactness grade and (*iii*) the density of aggregates. Up this point, we can affirm that just by changing the amount of nanoparticles loaded into the PVA, these are distributing differently. This will have a direct effect on the magnetic response, as will be discussed in the next section.

4. Magnetic analysis

To analyze the effect of the dipolar nanoparticle interactions on the magnetic response, a more detailed magnetic characterization is needed. To extract the values of the main magnetic parameters and to examine its progression as the nanoparticle concentration raise, different approaches were applied. Some of the used models are based on the superparamagnetic framework and the other ones, as the Interacting Superparamagnetic Model, consider the dipolar interactions. The studied parameters were the effective magnetic anisotropy energy density K_{eff}, mean magnetic moment $\langle\mu\rangle$, mean blocking temperature $\langle T_B\rangle$ and the relaxation time τ.

4.1. Magnetic field dependence of the magnetization of the PVA-IONPs

Fig. 4 shows M *vs.* H curves, taken at 5 K and 300 K, for all synthesized samples. Experimental curves of magnetic composites seem to be typical of systems with single domain nanoparticles, showing a coercive field close to zero for M *vs.* H curves measured at 300 K in accordance to a system in thermodynamic equilibrium [48], whereas for those measured at 5 K the coercive field shows larger values around 350 Oe for each sample. Magnetization does not reach saturation even under the maximum field of 20 kOe. To determine if the system in thermodynamic equilibrium behaves as a superparamagnetic one, the experimental curves where plotted as M/M_S *vs.* H/T (Supplementary material. Fig. 3.SI). As can be noted, the magnetization curves do not follow the superparamagnetic scaling law, which is an evidence of magnetic nanoparticle interactions.

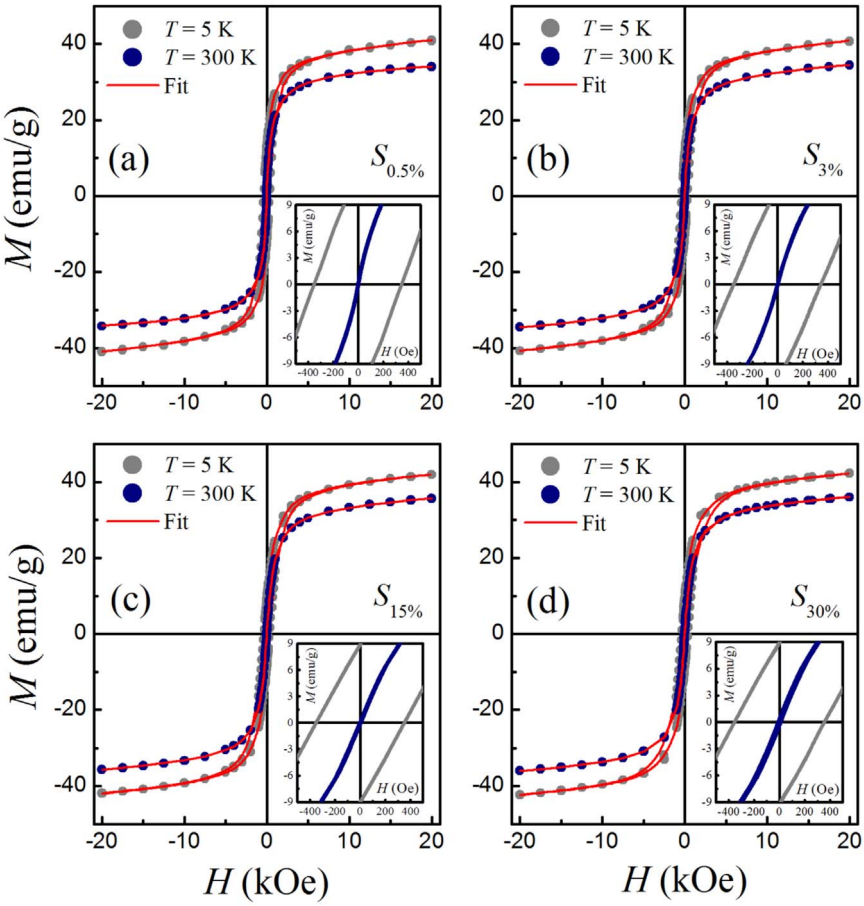

Fig. 4. Specific magnetization *vs.* applied field curves of magnetic composites. Measurements are shown for two selected temperatures: 5 K and 300 K. Specific mass magnetization is presented per IONPs mass. Red lines correspond to fits obtained from Langevin equation. *Insets*: magnification of the coercive field region. (For interpretation of the references to color in this figure legend, the reader is referred to the web version of this article.)

4.2. Temperature dependence of the specific saturation magnetization

For ordered magnetic systems, the temperature dependence of the spontaneous magnetization is studied in terms of collective excitations [49]. Such behavior is described by the so-called Bloch law and works very well for long-range ordered systems. However, some recent works report the use of a modified Bloch T^{α} law to study how the finite size effects affect the magnetization processes in small clusters and nanoparticle systems [50–53]. These effects are commonly associated with saturation magnetization departures from the usual Bloch $T^{3/2}$ temperature dependence [54]. Such modified law is given by:

$$M_S(T) = M_S(0)(1 - B'T^{\alpha}) + A_0 \exp(-T/T_{freezing}), \quad (3)$$

where $M_S(0)$ is the specific saturation magnetization when the temperature T approaches zero, B' is a variation of the Bloch constant (related to the exchange integral by $B' \sim 1/J$ [55]) for systems at the nanoscale, and α is the Bloch exponent. Normally in *bulk* ferromagnetic systems this latter quantity takes a value of 3/2, while in nanoscale systems a variation has been observed [56]. The second term is associated with the NPs surface layer that prevents magnetic saturation. This term is assumed to be characteristic of a surface in which all magnetic moments are disordered, so their contribution to the magnetization is zero at low fields, and it depends on the temperature at the surface in which the magnetic moments become frozen ($T_{freezing}$) and on the surface contribution at 0 K (A_0).

Despite the fact that the canonical Bloch law is based on the collective motion of the magnetic moments in ferromagnetic materials, it is possible to use its modified version in our systems to correlate a possible collective magnetic-moments behavior with the strengthening of dipole-dipole interactions between nanoparticles. It is important to point out that highly concentrated nanoparticle materials (almost or completely percolated) often display a similar magnetic behavior of bulk ferromagnetic materials [57].

To apply the mentioned model on our systems, we assume that the magnetic moments at the nanoparticle core are almost magnetically saturate at H=20 kOe. The $M_{H=20\ \mathrm{kOe}}$*vs.* T for each sample are presented in Fig. 5. Results indicate that for a given temperature, different magnetization values at H=20 kOe were reached. Commonly, this fact can be associated to different degrees of nanoparticle surface disorder. Nevertheless, on present samples such phenomena can be discarded because the IONPs retain the same surface features in all samples. This fact implies that the magnetic moment dynamics it is strongly affected by the dipolar interaction among nanoparticle magnetic cores. Another aspect to highlight is that in the concentrated nanocomposites, slightly larger values of $M_{H=20\ \mathrm{kOe}}$ are obtained, from which it is possible to infer that at high enough magnetic fields the magnetic dipolar interaction among magnetic cores would act to reinforce the core magnetic moment alignment with the external field.

To fit with Eq. (3), the parameter α was determined for the sample $S_{0.5\%}$ because weaker dipolar interactions are expected in this sample, and therefore one should follow the individual behavior of NPs. The obtained value of α=2 is in good agreement with results reported for systems composed of ferrites NPs with sizes of about 10 nm [50,58–61]. The deviation from the canonical Bloch law for bulk Fe_3O_4 (α=3/2 and $A_0 \approx A_{SURFACE} \approx 0$ in Eq. (3)) is mainly attributed to the reduction of the degrees of freedom of the NPs magnetic moment, *i.e.*, differences in the magnetic moment environment in a nanoparticle systems and its *bulk* counterpart implies different energy gaps to overcome in order to

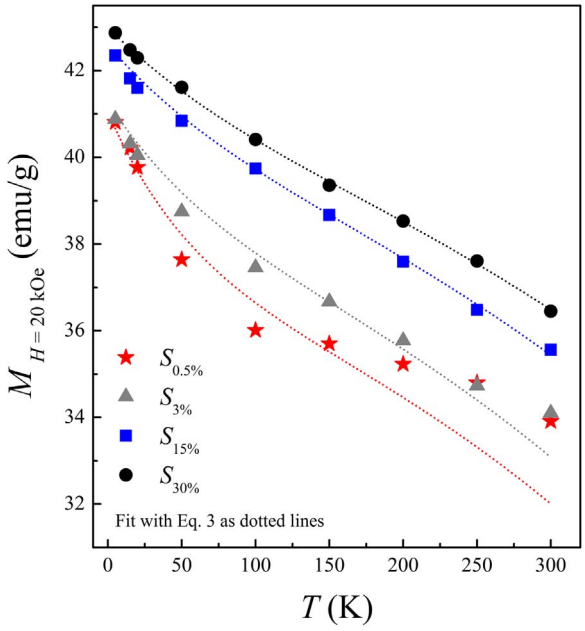

Fig. 5. Temperature dependence of $M_{H=20\ kOe}$ for all magnetic composites. Symbols represent the experimental data and the red solid line the fit to Eq. (3). (For interpretation of the references to color in this figure legend, the reader is referred to the web version of this article.)

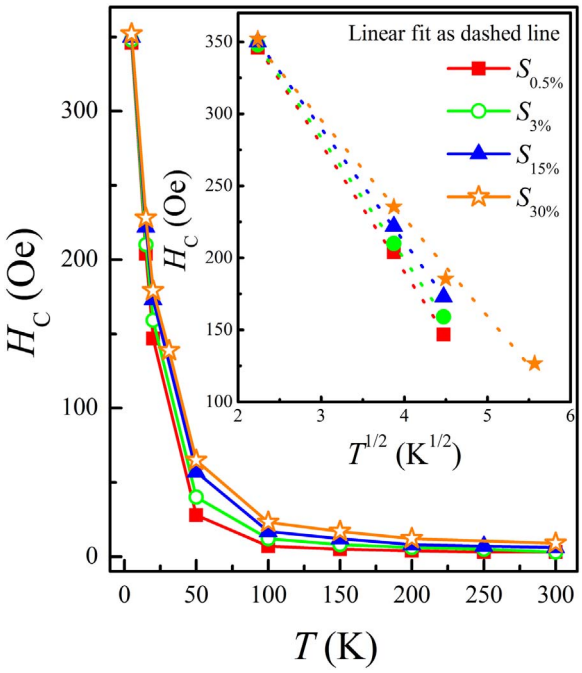

Fig. 6. Temperature dependence of H_C for the studied samples. *Inset*: coercive field follows the $T^{1/2}$ dependence.

trigger a collective movement of the magnetic moments [49,61,62].

A decrease in $M_{H=20\ kOe}$ with increasing temperature is seen for all samples, but for the diluted magnetic composites the decrease is more pronounced at lowest temperatures such that the $M_{H=20\ kOe}(T)$ behavior develops a concave shape. This behavior cannot be explained by a reduced or sample dependent parameter α [59,60], hence α was kept constant at a value of 2 in all settings. Analyzing the $M_{H=20\ kOe}(T)$ behavior of the concentrated samples ($S_{30\%}$ and $S_{15\%}$) the decrease at low temperatures is smooth, indicating that their behavior can be better represented by the Bloch theory. This means that both samples could present a superparamagnetic coupled or collective behavior when a field of about 20 kOe is applied at low temperatures, and this is consistent with the increase in dipolar interactions among NPs. In the two samples with lower NPs concentration ($S_{3\%}$ and $S_{0.5\%}$) the decrease of $M_{H=20\ kOe}$ at low temperatures is more pronounced, and the fit to Eq. (3) is not so good, pointing to a lower or null contribution of the collective magnetization processes.

Parameters obtained from $M_{H=20\ kOe}$ *vs.* T fit by means of Eq. (3) are summarized in Table 2. A feature to highlight is that A_0 is almost constant for all samples. This factor is related to the NPs disordered surface thickness [51]. Also, B' decreases with increasing NPs concentration from 1.3×10^{-6} K^{-2} for $S_{0.5\%}$ to 0.8×10^{-6} K^{-2} for $S_{30\%}$. Similar trends were reported by Bardeta et. al [61] and Franco et. al [63]. The B' value for this last sample is close to the one reported for bulk iron oxide systems (~1.58×10^{-6} K^{-2}) [50]. Those features indicate that the superparamagnetic behavior is screened due to dipolar interaction, and a possible ferromagnetic interaction between nanoparticle magnetic core moments becomes more relevant as the concentration of NPs increases. The evolution of freezing temperature $T_{freezing}$ is also consistent as it becomes larger when interactions increase.

Table 2
Fitting parameters obtained from $M_{H=20\ kOe}$ *vs.* T data using Eq. 3. *α was determined for the sample $S_{0.5\%}$ and was kept fixed in the fitting procedure for all other S samples.

Sample	$B'(\times10^{-6}\ K^{-2})$	A_0	$T_{freezing}$ (K)
$S_{0.5\%}$	1.3 (0.22)	5.0 (1.3)	63 (19)
$S_{3\%}$	1.2 (0.18)	4.3 (1.2)	80 (20)
$S_{15\%}$	1.0 (0.03)	3.9 (0.03)	99 (13)
$S_{30\%}$	0.8 (0.09)	3.8 (0.5)	108 (24)

4.3. Temperature dependence of coercivity

Fig. 6 shows the temperature dependence of the coercive field H_C. As expected, a significant increase of this parameter is observed in all samples as the temperature decreases. This behavior indicates the transition from a blocked regime at low T to non-blocked one at high temperatures. A slight larger value of H_C is detected at every temperature for the concentrated samples. Such behavior can be connected with a significant strengthening of dipole-dipole interactions [64].

$H_C(T)$ dependence for a system of non-interacting NPs in the blocked state can be modeled by [64]:

$$H_C = 0.48\frac{2K_{eff}^{H_C}}{\delta_{Fe_3O_4}M_S}\left[1-\left(\frac{T}{\langle T_B^{H_C}\rangle}\right)^{1/2}\right], \quad (4)$$

where $K_{eff}^{H_C}$ is the effective uniaxial anisotropy, $\delta_{Fe_3O_4}$ the magnetite density (assumed as 5.2 g/cm^3), M_S the saturation magnetization, and $\langle T_B^{H_C}\rangle$ the mean blocking temperature assuming a modest size dispersion (superscript indicates that the parameters are linked to Eq. (4)). According to the Néel-Arrhenius model, for an ideal system of single-domain magnetic nanoparticles in the blocked state, a linear dependence of H_C as function of $T^{1/2}$ is expected [65]. In our systems, such dependence was observed for $T < 20$ K in samples $S_{0.5\%}$, $S_{3\%}$, and $S_{15\%}$, while for the most concentrated one ($S_{30\%}$) the linear dependence of H_C with $T^{1/2}$ was found for a temperature range slightly broader ($T <$ 30 K). This difference indicates that the temperature range in which the magnetic NPs are blocked becomes wider in the most concentrated sample. Given the direct relationship between particle concentration and dipolar interaction strength, one can infer that the blocked window temperature is widened by the dipolar interaction effect. Such behavior is more obvious in the inset of Fig. 6, where H_C *vs.* $T^{1/2}$ was linearly fitted.

Considering the fact that at low temperatures H_C follow an almost

exact linear dependence with $T^{1/2}$ and assuming that the anisotropy constant as a temperature independent parameter in the linear fitting range [65,66], one can obtain the K_{eff}^{HC} values by extrapolating the linear fit to T=0. From this, a unique value of ~1.1×10^5 erg/cm^3 was found in all samples. This value is larger than the magnetocrystalline anisotropy of bulk Fe_3O_4 (6.4×10^4 erg/cm^3 [67]) as it is expected for systems at the nanoscale [16].

It is worth nothing that the obtained result of K_{eff}^{HC} must be used cautiously, just as a first approximation due to the framework behind the Eq. (4) is based on the conventional superparamagnetic theory, *i.e.*, it neglects features existing in any real sample, such as: particle size dispersion and the temperature dependence of the magnetic parameters involved [65], dipolar interaction effects [68], or possible effects associated to the Verwey transition, whose manifestation is linked to a structural disorder and could affect the anisotropy value in magnetite particles [69]. Despite the suppositions behind of the Eq. (4), the very reasonable value of K_{eff}^{HC} confirms the applicability of this approach for modest particle size dispersions and interactions [70–72].

4.4. Application of the Langevin theory and the Interacting Superparamagnetic Model

The magnetization of an assembly of polydisperse superparamagnetic nanoparticles, each one with a magnetic moment of magnitude μ can be described by the Langevin's equation [16,19]:

$$M(H,T) = n\int_0^\infty \mu L\left(\frac{\mu(H-H_C)}{k_BT}\right)f(\mu)d\mu, \quad (5)$$

being H_C the coercive field (assumed as small in comparison with the anisotropy field); n the number of superparamagnetic particles per mass unit; $L(x)$ the Langevin function; $f(\mu)$ the distribution of magnetic moments, assumed as lognormal type: $f(\mu)=\frac{1}{\sqrt{2\pi}\mu\sigma}\exp\left(-\frac{\ln(\mu/x_0)}{2\sigma^2}\right)$, with σ being the standard deviation and x_0 the median of the distribution.

By fitting Eq. (5) to the experimental $M(H)$ data (fitted curves are presented as continuous red lines at Fig. 4), the obtained mean magnetic moment $\langle\mu\rangle$ $\left(=x_0\exp\left(\frac{\sigma^2}{2}\right)\right)$ shows a non-physical increase with temperature, as shown in Fig. 7 (black spheres). The expected evolution of $\langle\mu\rangle$ with T it is to remain almost constant at low temperatures and to decrease as the temperature approaches the Curie limit (analogous to M_S behavior). This anomalous trend was observed by several authors and is often associated with the dipolar nanoparticle interaction effect on the on the magnetic behavior [16,25,29,73–75]. Consequently, the fitted values must be considered as *apparent*. For comparative purposes, in the sections below these values are re-labeled using the subscript 'AP'.

In order to understand the effect of dipolar interactions as a function of NPs concentration in the PVA matrix, we applied the model originally proposed by Allia *et. al.* [29]. This model, sometimes called T^* model or Interacting Superparamagnetic Model (ISP), was proposed as a phenomenological approach that considers that nanoparticle magnetic moments interact through dipolar type long-range fields, and the overall effect can be modeled by a fictitious temperature T^*, which should be added to the real temperature at the denominator of the Langevin function argument.

The new temperature, called apparent temperature, has the effect of slowing the approach to saturation and can be written as T_A=T+T^*, where T^* is related to the dipolar interaction energy through $\varepsilon_D = k_BT^*$. Then, the modified Lange vinfunction has the form:

$$M(H,T) = n_{CO}\int_0^\infty \mu_{CO} L\left(\frac{\mu_{CO}(H-H_C)}{k_B(T+T^*)}\right)f(\mu_{CO})d\mu_{CO}, \quad (6)$$

where 'CO' subscript refers to *corrected* fit values. To solve Eq. (6), it is necessary to determine T^*, what can be accomplished as follows: starting from the low field susceptibility that is given by $\chi_v = \frac{(N_{CO}\mu^2)}{3k_B(T+T^*)}$ and can be rewritten as:

$$\frac{\rho}{\chi_v} = 3k_BN_{CO}\left(\frac{T}{(\delta_{Fe_3O_4}M_S)^2}\right)+\beta, \quad (7)$$

where N_{CO} is the *corrected* number of magnetic moments of superparamagnetic particles per unit volume, which is related to the number of magnetic moments of superparamagnetic particles per mass unit through $N_{CO} = n_{CO}\delta_{Fe_3O_4}$, with $\delta_{Fe_3O_4}$ = 5.2g/cm^3 being the *bulk* magnetite density. ρ is a parameter introduced to consider the nanoparticle size distribution, which can be determined from the relationship among average values $\rho = \frac{\langle\mu_{CO}^2\rangle}{\langle\mu_{CO}\rangle^2} = \frac{\langle\mu_{AP}^2\rangle}{\langle\mu_{AP}\rangle^2}$[29]. The susceptibility χ_v is obtained from the low-field region of M *vs.* H curves (note that the units of M must be in emu/cm^3) and ρ is estimated from the lognormal distribution obtained from the parameters σ and $\langle\mu_{AP}\rangle$. By plotting $\frac{\rho}{\chi_v}$*vs.* $\frac{T}{M_S^2}$ and following the relationship between *apparent* and *corrected* parameters exposed in ref [29], one can obtain $\beta\left(=\frac{3k_BN_{CO}}{\delta_{Fe_3O_4}M_S^2}T^*\right)$ and therefore T^*.

A linear dependence of $\frac{\rho}{\chi_v}$ with $\frac{T}{M_S^2}$ is observed for higher temperatures (Supplementary material. Fig. 4.SI), that was properly fitted with a linear function in order to obtain the T^* values as well as the dipolar interaction energy ε_D. These values are registered in Table 3. Some trends can be highlighted, for example: (*i*) dipolar interaction energy becomes larger as the NPs concentration increases and, (*ii*) ε_D increases as the temperature becomes lower, indicating stronger dipolar interactions as the sample undergoes the transition between superparamagnetic and blocked regime.

Finally, with the calculated T^* values one can use Eq. (6) to fit the M *vs.* H curves and thus determine *corrected* magnetic parameters n_{CO} (or N_{CO}), σ and μ_{CO}. Fig. 7 shows the temperature dependence of $\langle\mu_{AP}\rangle$ and $\langle\mu_{CO}\rangle$. *Corrected* magnetic moments are higher than the *apparent* ones, as expected. These results agree with the Monte Carlo simulations performed by Kechrakos et al. [76], who proposed that dipolar interactions act minimizing the magnetic response of granular magnetic systems. Remarkably, in concentrated systems, $\langle\mu_{CO}\rangle$ first increases at low temperature before it then starts the expected decreasing trend. Such maximum can be due to a restriction of the ISP model, especially at those temperatures in which a significant percentage of nanoparticles are still blocked. Unlike the results obtained from the classical Langevin equation, where all $\langle\mu_{AP}\rangle$ values are all of the same order of magnitude for every samples, in those obtained from the ISP model there is a strong growth of $\langle\mu_{CO}\rangle$ with NPs concentration, as shown in Fig. 7 and Table 4. The *corrected* number of magnetic moments per unit volume in superparamagnetic state (N_{CO}) is also listed in Table 4. In all samples, a higher value of this parameter is observed as the temperature increases, which is expected because the increase in temperature causes more nanoparticles to pass from the blocked state to the non-blocked one. In summary, based on obtained parameters it is possible to infer that for the concentrated nanocomposites, the ISP model *interprets* that there are fewer but larger magnetic moments per unit volume, which is in agreement with the formation of more compacted NPs aggregates (as it is seen by SAXS) and to the potential coherent collective behavior, as was inferred by the analysis of the thermal variations of the saturation magnetization using the modified Bloch law.

4.5. Temperature dependence of the AC magnetic susceptibility

From the results of AC magnetic susceptibility studies, we determine the empirical parameter known as the Mydosh parameter Φ [77]. From this, the strengthening of the interparticle interactions can be qualitatively followed. Such parameter can be calculated from the imaginary part of the AC susceptibility according to the equation:

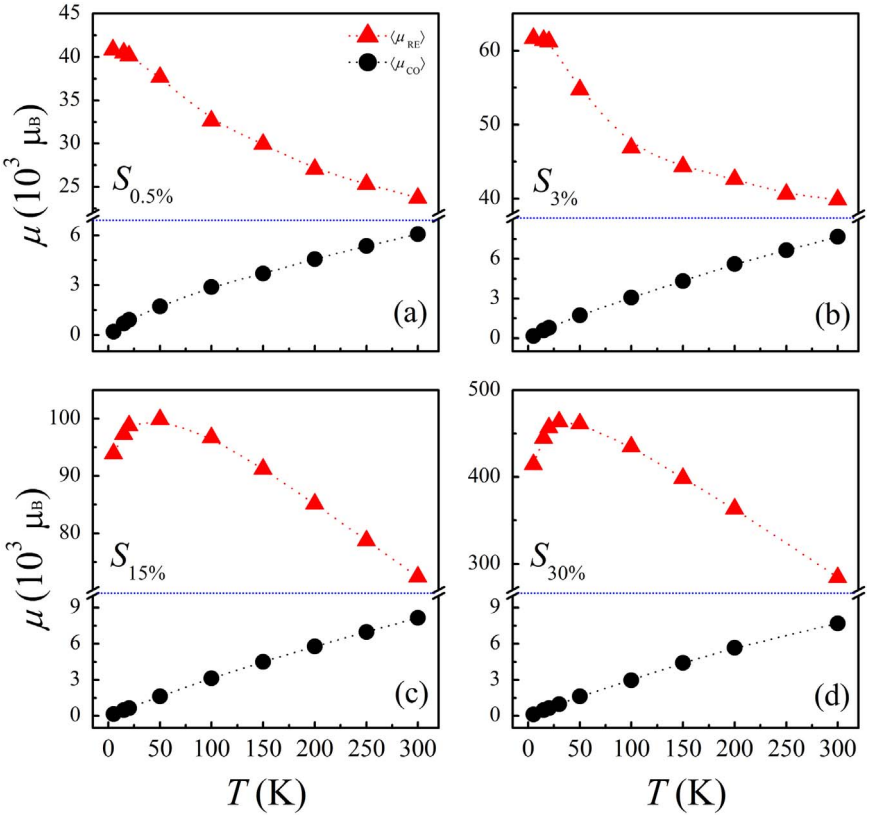

Fig. 7. Temperature dependence of *apparent* (black symbols) and *corrected* (red symbols) magnetic moments for all studied magnetic composites. (For interpretation of the references to color in this figure legend, the reader is referred to the web version of this article.)

$\Phi = \frac{\Delta T_{MAX}^{\chi''}}{T_{MAX}^{\chi''}\Delta log(f)}$, being $\Delta T_{MAX}^{\chi''}$ the relative variance measured in the $\Delta log(f)$[78], with f as the measuring frequency (temperature dependence of the AC magnetic susceptibility is shown in the Supplementary material. Fig. 5.SI). The calculated Φ value for the most diluted sample ($S_{0.5\%}$) is close to the value expected for weakly or non-interacting nanoparticle systems (~0.1) [50,70,78], while for the intermediate samples ($S_{3\%}$ and $S_{15\%}$), Φ ranging between 0.7–0.8, which is characteristic of nanoparticle systems with intermediate interactions [79] (see Table 5). For sample $S_{30\%}$, Φ=0.06, result that could be related to the manifestation of strong interparticle interactions.

According to the superparamagnetic theory, the nanoparticle magnetic moment relaxation time τ_0 must take values of between 10^{-9} and 10^{-10} s. There are two common approaches to extract the relaxation time: these are the Néel-Arrhenius (N-A) and the Vogel-Fulcher (V-F) laws. By using the N-A law, several works reports unphysical values for relaxation time, arguing that the nanoparticle interactions effects lead to underestimate the reversion time of the magnetic moment [50,53,70,80]. In our samples, the use of the N-A law also leads to obtain low values without physical meaning. The results obtained by N-A law are displayed at the supporting information. With the aim of to consider the dipolar interactions among nanoparticles, the V-F law, as the ISP model, uses a fictitious temperature to simulate the effect of long-range dipolar forces. The V-F law is given by:

$$\tau = \tau_0^{VF} \exp\left[\frac{K_{eff}^{VF}\ V}{k_B(T - T_0^{VF})}\right], \tag{8}$$

where τ is the measuring time window, τ_0^{VF} is the relaxation extracted from V-F law, K_{eff}^{VF} is the effective anisotropy constant, V is the nanoparticle volume and T_0^{VF} is the fictitious temperature above mentioned, that is directly proportional to the strength of interparticle dipolar interaction (VF superscripts indicates that the parameters are linked with V-F law). The best fitting results according to V-F law are presented in Fig. 8. and registered in Table 5. As can be seen, suitable relaxation time values around of ~10^{-9} s were found for all samples. It is also noticed that the magnitude of the anisotropy (~10^5 erg/cm^3) is closer to that previously extracted from de coercivity analysis and, are good agreement with those found for systems composed of monodomain magnetic nanoparticles [70]. Moreover, the expected tendency of T_0^{VF} was found, *i.e.*, it increases proportionally with the nanoparticle concentration, which is in good agreement with the systematically strengthening of the dipolar magnetic interactions.

Table 3
T^* values obtained by means of Eq. (7). Dipolar energy (ε_D) values are also presented.

	$S_{0.5\%}$		$S_{3\%}$		$S_{15\%}$		$S_{30\%}$	
T (K)	T^*(K)	ε_D (10^{-13} erg)	T^*(K)	ε_D (10^{-13} erg)	T^*(K)	ε_D (10^{-13} erg)	T^*(K)	ε_D (10^{-13} erg)
20	1063	1.5	1605	2.2	3122	4.3	14,488	20.0
50	1048	1.4	1571	2.2	3067	4.2	14,217	19.6
100	1018	1.4	1529	2.1	2990	4.1	13,886	19.1
200	931	1.3	1409	2.0	2748	3.8	12,776	17.6
300	799	1.1	1219	1.7	2365	3.3	11,028	15.2

Table 4
Best fitting parameters for samples $S_{0.5\%}$, $S_{3\%}$, $S_{15\%}$ and $S_{30\%}$ obtained from ISP model for selected T values.

	$S_{0.5\%}$			$S_{3\%}$			$S_{15\%}$			$S_{30\%}$		
T (K)	N_{CO} (10^{17} cm^{-3})	σ	$\langle\mu_{CO}\rangle$ ($10^3\mu_B$)	N_{CO} (10^{17} cm^{-3})	σ	$\langle\mu_{CO}\rangle$ ($10^3\mu_B$)	N_{CO} (10^{17} cm^{-3})	σ	$\langle\mu_{CO}\rangle$ ($10^3\mu_B$)	N_{CO} (10^{16} cm^{-3})	σ	$\langle\mu_{CO}\rangle$ ($10^3\mu_B$)
20	4.2	0.7	40.2	3.2	0.5	61.2	2.2	0.3	98.8	4.8	0.3	457
50	5.7	1.10	37.7	3.7	0.81	54.7	2.1	0.37	99.9	4.7	0.39	461
100	5.7	1.49	32.6	4.4	1.01	46.9	2.2	0.52	96.7	5.2	0.60	435
200	7.8	1.29	27.1	4.6	1.04	42.6	2.4	0.66	85.1	5.7	0.67	364
300	7.8	1.22	23.7	4.6	0.98	39.9	2.7	0.72	72.4	6.8	0.77	284

Table 5
Parameters τ_0^{VF}, K_{eff}^{VF} and T_0^{VF} obtained from the fitting of $\ln(\tau)$ vs. $1/T_{MAX}^{\chi''}$ according to Vogel – Fulcher law for samples $S_{0.5\%}$, $S_{30\%}$, $S_{15\%}$ and $S_{30\%}$. Mydosh parameter Φ is also registered.

Sample	τ_0^{VF} (s)	K_{eff}^{VF} (erg/cm^3)	T_0^{VF} (K)	Φ
$S_{0.5\%}$	8.1×10^{-9}	1.9×10^5	48.3	0.09
$S_{3\%}$	1.2×10^{-9}	2.2×10^5	50.4	0.08
$S_{15\%}$	3.3×10^{-9}	8.8×10^5	71.2	0.07
$S_{30\%}$	1.1×10^{-9}	8.3×10^5	76.2	0.06

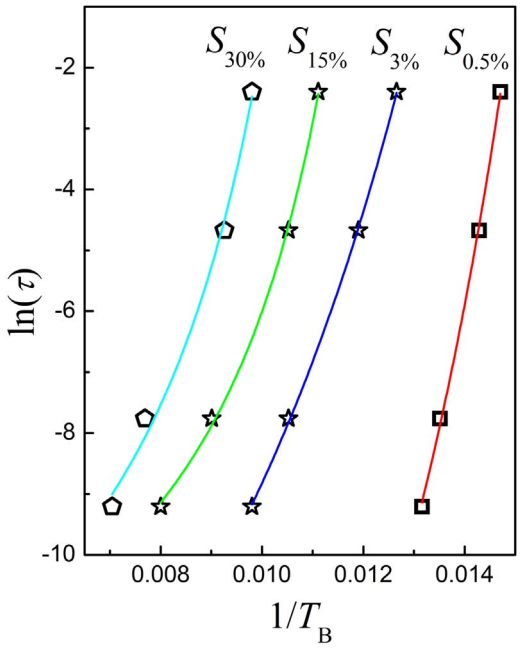

Fig. 8. Plots of $\ln(\tau)$ vs. $\frac{1}{T_{MAX}^{\chi''}}$ ($T_{MAX}^{\chi''}$ is the peak temperature of the imaginary component at each measured frequency). The full line corresponds to the fit according to Vogel–Fulcher law.

4.6. Zero-field-cooling and field-cooling curves analysis

Owing to the larger sensitivity of the zero-field-cooling (ZFC) and field-cooling (FC) magnetization curves, these are very useful experimental measurements to observe smooth changes between similar systems. Despite that the framework behind these curves is based on highly ideal systems, in the remaining sections we will use the information obtained from these curves, together with the previous structural and magnetic results, to check its consistency against experimental data obtained from diluted and concentrated systems studied here.

Fig. 9 shows the ZFC/FC experimental curves (symbols) of the studied magnetic composites. As can be clearly seen, for increasing the nanoparticle concentration in PVA matrices, the maxima of the experimental ZFC curves (T_{MAX}^{ZFC}) shift to higher temperatures.

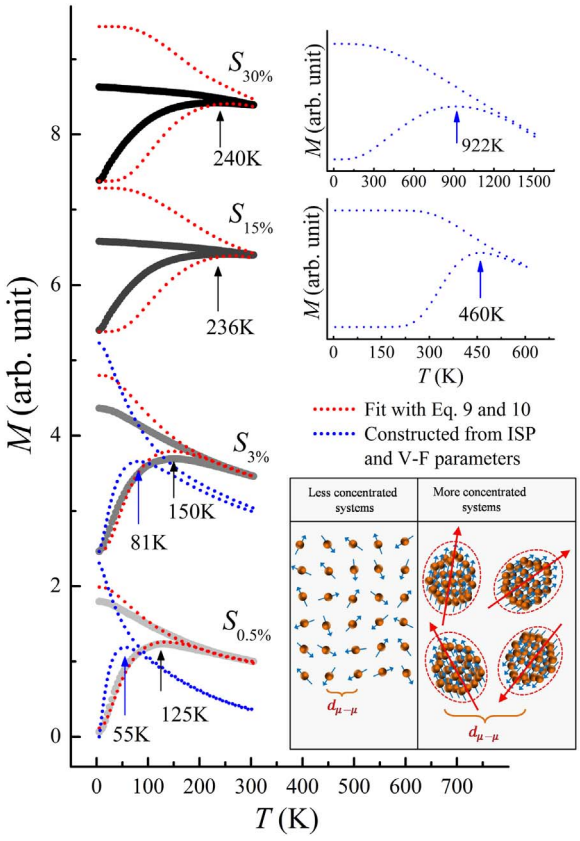

Fig. 9. ZFC/FC curves of all samples taken in a magnetic field of 50 Oe. Red dashed line indicates the fitting curves obtained from Eqs. 9 and 10. Blue dashed line denotes the ZFC/FC curves constructed using the parameters obtained from ISP and Vogel-Fulcher models. The constructed curves of the samples $S_{15\%}$ and $S_{30\%}$ are plotted in a different layer for scaling reasons. (For interpretation of the references to color in this figure legend, the reader is referred to the web version of this article.)

Regarding to the overall shape of the ZFC/FC curves, one can see that those samples with lower nanoparticle concentration ($S_{0.5\%}$ and $S_{3\%}$) are characteristic of weakly interacting superparamagnetic systems [18,19,25,26,81–83]. On the other hand, the shape displayed by the concentrated samples ($S_{15\%}$ and $S_{30\%}$) presents a broader peak, which is representative of systems with strong or moderate interparticle dipolar interactions [23,83,84]. These features are new confirmation that the magnetic response of the studied magnetic composites can be tuned by varying the nanoparticle concentration into the PVA matrices.

Fig. 9 also shows that for all samples, the irreversibility temperature is different from the maximum displayed by the ZFC curves, because to a distribution of blocking temperatures [18,82]. That distribution of blocking temperatures $f(T_B)$, can be obtained from the derivative $\frac{d}{dT}(M_{ZFC} - M_{FC})$ [85,86] (Fig. 6.SI). From it, the mean blocking temperature $\langle T_B\rangle$ was extracted to then use it to calculate the anisotropy constant through $K_{eff}^{\langle T_B\rangle} = \frac{25k_B\langle T_B\rangle}{V}$ [18,87] (the superscript indicates that the anisotropy constant was obtained using $\langle T_B\rangle$). Using that functional

Table 6.
Calculated anisotropy constant $K_{eff}^{\langle T_B\rangle}$. Parameters K_{eff}^{Fit}, T_B, τ_0 (defined in the text) obtained from the ZFC/FC curves fitted with Eqs. (9) and (10). Noted that the superscript indicates that the anisotropy constant was obtained using $K_{eff}^{\langle T_B\rangle} = 25k_B\langle T_B\rangle/V$ or from the ZFC-FC fitting procedure as the case.

Sample	T_{MAX}^{ZFC} (K)	$K_{eff}^{\langle T_B\rangle}$ (10^5 erg/cm^3)	Fitted parameters obtained using Eqs. (9) and (10)		
			K_{eff}^{Fit} (10^5 erg/cm^3)	T_B (K)	τ_0 (s)
$S_{0.5\%}$	125	6.3	1.1	73	1.4×10^{-11}
$S_{3\%}$	150	8.5	1.2	82	1.1×10^{-12}
$S_{15\%}$	236	9.1	2.1	160	9.3×10^{-15}
$S_{30\%}$	240	11.1	2.4	163	8.2×10^{-16}

relation, we obtained $K_{eff}^{\langle T_B\rangle}$=6.3×10^5 erg/cm^3 for the most diluted sample, and $K_{eff}^{\langle T_B\rangle}$=1.1×10^6 erg/cm^3 for the most concentrated sample (all values are registered in Table 6). It is clear that an increase in $\langle T_B\rangle$ brings a proportional growth of $K_{eff}^{\langle T_B\rangle}$. Therefore, for concentrated composites, in which the mean blocking can be distorted by the nanoparticle interaction action, the obtained anisotropy constant values are restricted by this fact. These results corroborate previous studies that indicated that spurious parameters could be obtained from magnetic data, if the effect of interactions and a proper analysis of the nanostructure are not considered [29,82,84].

Comparing the effective anisotropy values obtained for the diluted composites it is possible to note than those acquired from V-F law (1.9×10^5 and 2.2×10^5 erg/cm^3 for samples $S_{0.5\%}$ and $S_{3\%}$, respectively) and from the extrapolation of the linear fit of H_C*vs.* $T^{1/2}$ (1.1×10^5 erg/cm^3 for $S_{0.5\%}$ and $S_{3\%}$) are in good agreement. The slight differences could be related to temperature threshold in which the approaches act. *i.e.* the experimental data used in the V-F analysis came from an AC measure which was performed for a temperature range between 5 K and 300 K, this means the anisotropy value extracted from this approach carries information of both blocked and superparamagnetic states, while the anisotropy value obtained from the $H_C(T)$ emerges from a DC measures and it is restricted to lower temperatures, particularly for $T < T_B$ ranges in which the larger nanoparticles maintain their blocked state.

To complement the above results, we fit the ZFC/FC data of all samples using the superparamagnetic model for non-interacting particles. Such model stipulates that the zero-field-cooled magnetization of a system of noninteracting particles with a distribution of blocking temperatures is [18,81,82,88–91]:

$$M_{ZFC}(T) = \frac{M_S^2 H}{3K_{eff}}\left[\ln\left(\frac{\tau_m}{\tau_0}\right)\frac{1}{T}\int_0^T T_B f(T_B)dT_B + \int_T^\infty f(T_B)dT_B\right], \quad (9)$$

where $f(T_B)$ is the distribution of blocking temperatures (assumed as a lognormal distribution according to the already obtained information); M_S is the saturation magnetization; H is the applied magnetic field; T and T_B are the absolute and blocking temperature, respectively; K_{eff} is the anisotropy constant and; τ_m and τ_0 are the measurement and characteristic time, respectively. The first integral denotes the contribution of the superparamagnetic particles, whereas the second corresponds to the blocked ones. Regarding M_{FC}, the nanoparticles contribution to the magnetization below T_B is not randomly orientation of moments. In this case it is assumed to be the magnetization value at the blocking temperature [18,82]. Thus, one can write the FC magnetization as

$$M_{FC}(T) = \frac{M_S^2 H}{3K_{eff}}\ln\left(\frac{\tau_m}{\tau_0}\right)\left[\frac{1}{T}\int_0^T T_B f(T_B)dT_B + \int_T^\infty f(T_B)dT_B\right]. \quad (10)$$

For fitting purposes, in the above expressions H=50 Oe, τ_m=100 s and M_S (obtained from M *vs.* H curve of at T=300 K) were held fixed. The fits for the experimental data according to Eqs. 9 and 10 are shown in Fig. 9 (red dashed line). As can be seen, for the diluted samples ($S_{0.5\%}$ and $S_{3\%}$) the fitted curves show good agreement with the experimental data, whereas for the concentrated samples ($S_{15\%}$ and $S_{30\%}$) the fitted curves do no match with the experimental ones, even considering they are the best fits obtained in the framework of the non-interacting superparamagnetic model. From these fits the anisotropy, blocking temperature and relaxation time were obtained (see Table 6).

Examining these results it is possible to note that for diluted samples, the fitted values of K_{eff}^{Fit} match in the order of magnitude with those presented in previous magnetic sections, while for concentrated systems this parameter keep the tendency to increase. Therefore, the obtained parameters associated to the concentrated samples and presented in the currently section must be considered as a qualitative approximation, because the used approaches ($K_{eff}^{\langle T_B\rangle} = \frac{25k_B\langle T_B\rangle}{V}$ or M_{ZFC}-M_{FC} equations) are founded on the framework of the non-interacting superparamagnetic theory.

The characteristic time (τ_0) is another significant parameter obtained from the previous analysis. For samples $S_{0.5\%}$ and $S_{3\%}\tau_0$ has value of 1.4×10^{-11} s and 1.1×10^{-12} s, respectively. It is noteworthy that these values are in the expected range for weakly interacting superparamagnetic systems [90]. On the other hand, for the concentrated samples, unphysical smaller values were found: τ_0=9.3×10^{-15} s and τ_0=8.2×10^{-16} s for samples $S_{15\%}$ and $S_{30\%}$, respectively. In summary, we can affirm that the two diluted samples are closer to the superparamagnetic behavior and can be treated accordingly, which is not the case of the concentrated samples studied here. It is also notable that the τ_0 displays unphysical values for samples $S_{15\%}$ and $S_{30\%}$ when it is determined from the Néel-Arrhenius formula (see Supporting Information).

4.7. A re-interpretation based on the construction of the ZFC/FC curves from ISP and V-F results

We have shown that the classical superparamagnetic theory can be applied on the diluted samples to obtain coherent values of the magnetic parameters. Nonetheless, by using models that consider interactions between magnetic entities (for example ISP model or the Vogel-Fulcher law) such values can be refined. For samples $S_{15\%}$ and $S_{30\%}$, in which the strength of the magnetic interparticle interactions is higher, using such models leads to inconsistent results; for example, nanoparticle sizes and magnetic moments several times larger than the real ones, un-physical values for the moment relaxation time and overestimated values for the anisotropy.

In order to visualize how good those current models are to depict a real nanogranular material like our magnetic composites, we used data obtained from ISP model and Vogel-Fulcher law, which gave the most accurate values, to rebuild the ZFC-FC curves and compared them to the experimental ones. To do this, we simulate the Eqs. (9) and (10) using the obtained parameters $\langle\mu_{CO}\rangle$, N_{CO}, τ_0^{VF} and K_{eff}^{VF}, and the experimental parameters H and τ_m (50 Oe and 100 s, respectively).

First we must calculate the magnetic volume (V^{ISP}) of the entity with a magnetic moment equal to the *corrected* one obtained from the ISP analysis ($\langle\mu_{CO}\rangle_{T=300K}$). Therefore, we used the theoretical magnetic moment of a single magnetite nanoparticle with a diameter of 8.4 nm (corresponding volume 3.1×10^{-19} cm^3 and $\mu_{theoretical} \approx 21.6\text{x}10^3\mu_B$). Such magnetic volume can be calculated by $V^{ISP} = V_{1NP}\frac{\langle\mu_{CO}\rangle_{T=300K}}{\mu_{theoretical}}$ and their equivalent blocking temperature can be determined from the functional definition: $T_B^{ISP/VF} = K_{eff}^{VF}V^{ISP}/k_B\ln\left(\frac{\tau_m}{\tau_0^{VF}}\right)$ (all values are registered in Table 7). The saturation magnetizations can be calculated by $M_S^{ISP} = N_{CO}\langle\mu_{CO}\rangle$. Based on the above results, we assume a lognormal distribution and owing to the direct proportionality among the blocking temperature, the nanoparticle volume and its magnetic moment, we assume that the σ obtained from the lognormal magnetic moment distribution (from ISP results at T=300 K) can be used to build a lognormal distribution of blocking temperatures.

Table 7
Used values for the construction of the ZFC/FC curves and the calculated distance between magnetic entities ($d_{\mu-\mu}$) from the ISP model. Superscripts indicate that the values were obtained from the ISP and/or V-F analysis.

Sample	$\frac{\langle\mu_{CO}\rangle_{T=300K}}{\mu_{theoretical}}$	V^{ISP} (cm^3)	$T_B^{ISP/VF}$ (K)	$d_{\mu-\mu}$ (nm)
$S_{0.5\%}$	1.1	4.1×10^{-19}	25	7
$S_{3\%}$	1.9	7.2×10^{-19}	46	9
$S_{15\%}$	3.5	1.3×10^{-18}	343	14
$S_{30\%}$	13.2	5×10^{-18}	1190	21

The constructed ZFC/FC curves are shown in Fig. 9 (blue dashed lines). Even though these curves are built from values obtained from the analysis of *M vs. H* curves and AC measurements there is remarkable agreement between them and the experimental results for the samples $S_{0.5\%}$ and $S_{3\%}$. This is not the case for samples $S_{15\%}$ and $S_{30\%}$, which do not match with the experimental data and whose shape and the position temperature peak can be associated with larger monodomain magnetic entities.

Since the ZFC/FC curves describe the thermal dependence of the magnetization of single magnetic entities and noticing that the $\langle\mu_{CO}\rangle_{T=300K}/\mu_{theoretical}$ ratio is around 1 for the most diluted sample. We can conclude that the magnetic volume of a single magnetic entity in the sample $S_{0.5\%}$ is almost the same as the theoretical one of a single magnetite nanoparticle of 8.4 nm. Reason for which, the experimental and constructed ZFC/FC curves display a distinctive correspondence.

On the other hand, the increase in the nanoparticle concentration carries with it a progressive divergence between the experimental and constructed ZFC/FC curves as well as among the calculated magnetic volume of a single entity and the nanoparticle volume. Such that for sample $S_{3\%}$ the magnetic volume of a single entity is 1.9 times the volume of a single magnetite nanoparticle of 8.4 nm and for the concentrated samples $S_{15\%}$ and $S_{15\%}$ this is 3.5 and 13.2 times larger, respectively.

Bearing in mind the phenomenological basis of the ISP model and remembering that from SAXS analysis was detected a gradual growing of aggregates, being these more compact at larger nanoparticle concentration. In summary we can say that for the concentrated systems presented here, the ISP model identifies aggregates of nanoparticles as single and larger magnetic entities, who have a volume and a unique magnetic moment equivalent to the sum of the NPs volumes and NPs magnetic moments that constitute every aggregate. A schematic representation of the hypothesis proposed here is shown in the inset of Fig. 9.

5. Conclusions

Two diluted and two concentrated granular superparamagnetic composites, synthesized by loading different amounts of magnetite nanoparticles in polymeric matrices, were used to better understand the crossover between weak interacting and collective behavior, mediated by dipolar interaction effects.

The superparamagnetic and the interacting superparamagnetic models as well as the Vogel-Fulcher and Bloch laws, among others approaches, were employed in order to get a complete picture of the interaction strengthening effect on the magnetic response. The obtained results reveal different scenarios for diluted and concentrated nanocomposites. These suggest that for diluted composites, the magnetic nanoparticles are weakly interacting and the magnetic behavior can be associated to the individual nanoparticles comportment. Whereas in concentrated samples the system progresses to interacting superparamagnetic or collective behavior due to the fact that interactions become more relevant.

Several approaches were employed to obtain the most representative magnetic parameters, some of them are the anisotropy constant and the relaxation time. Remarkably that for concentrated samples, larger and possibly overestimated values of K_{eff} were found, while unphysical and lower values were detected for τ_0. We found that the mentioned inconsistencies should be related to the models restrictions in the case of strong magnetic interactions. Then, Vogel-Fulcher law was used to determine a more accurate values of these two parameters; obtaining coherent values of approximately K_{eff} ~10^5 erg/cm^3 and τ_0~10^{-9} s for all samples. Considering the framework behind the ISP model and the obtained results, it is possible to conclude that for the concentrated nanocomposites studied here, this model describes compacted agglomerates of nanoparticles as if they were single magnetic entities. This fact was also reflected in the simulated ZFC/FC curves.

Acknowledgement

O. M. L., D. M., and M. K. acknowledge FAPESP (2014/26672-8, 2011/01235-6 and 2011/02356-11), P. T. and L. M. S. thank CONICET and ANPCyT, for financial support. LNLS - CNPEM is acknowledged for XAS measurements (XAFS1–17726). We thank M. González Batiller for FT-IR measurements. O. M. L. would like to thank COLCIENCIAS, Colombia.

Appendix A. Supporting information

Supplementary data associated with this article can be found in the online version at doi:10.1016/j.jmmm.2016.12.019.

References

[1] A.C. Balazs, T. Emrick, T.P. Russell, Nanoparticle polymer composites: where two small worlds meet, Science 314 (2006) 1107–1110.
[2] R.A. Vaia, J.F. Maguire, Polymer nanocomposites with prescribed morphology: going beyond nanoparticle-filled polymers, Chem. Mater. 19 (2007) 2736–2751.
[3] G. Filipcsei, I. Csetneki, A. Szilágyi, M. Zrínyi, Magnetic field-responsive smart polymer composites, Adv. Polym. Sci. 206 (2007) 137–189.
[4] T.-Y. Liu, S.-H. Hu, T.-Y. Liu, D.M. Liu, S.Y. Chen, Magnetic-sensitive behavior of intelligent ferrogels for controlled release of drug, Langmuir 22 (2006) 5974–5978.
[5] P. Tartaj, M.P. Morales, S. Veintemillas-Verdaguer, T. González-Carreño, C.J. Serna, The preparation of magnetic nanoparticles for applications in biomedicine, J. Phys. D: Appl. Phys. 36 (2003) R182–R197.
[6] Q.A. Pankhurst, J. Connolly, S.K. Jones, J.J. Dobson, Applications of magnetic nanoparticles in biomedicine, J. Phys. D: Appl. Phys. 36 (2003) R167–R181.
[7] C.C. Berry, A.S.G. Curtis, Functionalisation of magnetic nanoparticles for applications in biomedicine, J. Phys. D: Appl. Phys. 36 (2003) R198–R206.
[8] C.C. Berry, Possible exploitation of magnetic nanoparticle–cell interaction for biomedical applications, J. Mater. Chem. 15 (2005) 543–547.
[9] H. Matsuyama, M. Teramoto, H. Urano, Analysis of solute diffusion in poly(vinyl alcohol) hydrogel membrane, J. Membr. Sci. 126 (1997) 151–160.
[10] D.J.T. Hill, A.K. Whittaker, Zainuddin, Water diffusion into radiation crosslinked PVA–PVP network hydrogels, Radiat. Phys. Chem. 80 (2011) 213–218.
[11] D. Mawad, R. Odell, L.A. Poole-Warren, Network structure and macromolecular drug release from poly(vinyl alcohol) hydrogels fabricated via two crosslinking strategies, Int. J. Pharm. 366 (2009) 31–37.
[12] C. Hassan, N. Peppas, Structure and applications of poly(vinyl alcohol) hydrogels produced by conventional crosslinking or by freezing/thawing methods, Adv. Polym. Sci. 153 (2000) 37–65.
[13] O. Moscoso-Londoño, J.S. Gonzalez, D. Muraca, C.E. Hoppe, V.A. Alvarez, A. López-Quintela, et al., Structural and magnetic behavior of ferrogels obtained by freezing thawing of polyvinyl alcohol/poly(acrylic acid) (PAA)-coated iron oxide nanoparticles, Eur. Polym. J. 49 (2013) 279–2289.
[14] S. Kayal, R.V. Ramanujan, Doxorubicin loaded PVA coated iron oxide nanoparticles for targeted drug delivery, Mater. Sci. Eng. 30 (2010) 484–490.
[15] T.-Y. Liu, S.-H. Hu, K.-H. Liu, D.-M. Liu, S.-Y. Chen, Study on controlled drug permeation of magnetic-sensitive ferrogels: effect of Fe_3O_4 and PVA, J. Control. Release 126 (2008) 228–236.
[16] P. Mendoza Zélis, D. Muraca, J.S. Gonzalez, G.A. Pasquevich, V.A. Alvarez, K.R. Pirota, et al., Magnetic properties study of iron-oxide nanoparticles/PVA ferrogels with potential biomedical applications, J. Nanopart. Res 15 (2013) 1613.
[17] P. Allia, P. Tiberto, M. Coisson, A. Chiolerio, F. Celegato, F. Vinai, et al., Evidence for magnetic interactions among magnetite nanoparticles dispersed in photoreticulated PEGDA-600 matrix, J. Nanopart. Res. 13 (2011) 5615–5626.
[18] M. Knobel, W.C. Nunes, L.M. Socolovsky, E. De Biasi, J.M. Vargas, J.C. Denardin, Superparamagnetism and other magnetic features in granular materials: a review on ideal and real systems, J. Nanosci. Nanotechnol. 8 (2008) 2836–2857.
[19] L.M. Socolovsky, O. Moscoso-Londoño, Consequences of magnetic interactions

phenomena in granular systems, in: S.K. Sharma (Ed.)Complex Magnetic Nanostructures - Synthesis, Assembly and Applications, Springer, Rio de Janeiro, 2016.
[20] L.M. Socolovsky, C.L.P. Oliveira, J.C. Denardin, M. Knobel, I.L. Torriani, Nanostructure of granular Co-SiO_2 thin films modified by thermal treatment and its relationship with the giant Hall effect, Phys. Rev. B 72 (2005) 184423.
[21] L.M. Socolovsky, F.H. Sánchez, P.H. Shingu, Magnetic structure of Fe_xCu_{100-x} magnetoresistive alloys produced by mechanical alloying, Hyperfine. Interact. 133 (2001) 47–52.
[22] M. Hillenkamp, G. Di Domenicantonio, C. Félix, Interaction effects in dilute cluster-assembled magnetic nanostructures, Phys. Rev. B 77 (2008) 014422.
[23] S. Bedanta, W. Kleemann, Supermagnetism, J. Phys. D: Appl. Phys. 42 (2009) 013001.
[24] E. Lima, E. De Biasi, M. Vasquez Mansilla, M.E. Saleta, M. Granada, H.E. Troiani, et al., Heat generation in agglomerated ferrite nanoparticles in an alternating magnetic field, J. Phys. D: Appl. Phys. 46 (2013) 045002.
[25] J.M. Vargas, W.C. Nunes, L.M. Socolovsky, M. Knobel, D. Zanchet, Effect of dipolar interaction observed in iron-based nanoparticles, Phys. Rev. B 72 (2005) 184428.
[26] J.M. Vargas, L.M. Socolovsky, M. Knobel, D. Zanchet, Dipolar interaction and size effects in powder samples of colloidal iron oxide nanoparticles, Nanotechnology 16 (2005) S285–S290.
[27] S. Mørup, E. Tronc, Superparamagnetic relaxation of weakly interacting particles, Phys. Rev. Lett. 72 (1994) 3278–3281.
[28] L. Dormann, D. Fiorani, E. Tronc, On the models for interparticle interactions in nanoparticle assemblies: comparison with experimental results, J. Magn. Magn. Mater. 202 (1999) 251–267.
[29] P. Allia, M. Coisson, P. Tiberto, F. Vinai, M. Knobel, M.A. Novak, et al., Granular Cu-Co alloys as interacting superparamagnets, Phys. Rev. B 64 (2001) 144420.
[30] S. Oyarzún, A. Tamion, F. Tournus, V. Dupuis, M. Hillenkamp, Size effects in the magnetic anisotropy of embedded cobalt nanoparticles: from shape to surface, Sci. Rep. 5 (2015) 14749.
[31] Y.S. Kang, S. Risbud, J.F. Rabolt, P. Stroeve, Synthesis and characterization of nanometer-size Fe_3O_4 and γ-Fe_2O_3 particles, Chem. Mater. 8 (1996) 2209–2211.
[32] A.C.Larson, R.B.V.Dreele, *General Structure Analysis System* (*GSAS*)(Los Alamos National Laboratory Report, 2000.
[33] B.H. Toby, EXPGUI, a graphical user interface for GSAS, J. Appl. Cryst. 34 (2001) 210–213.
[34] J. Kohlbrecher, A Program for Fitting Simple Structural Models to Small Angle Scattering Data, Paul Scherrer Institute Laboratory for Neutron Scattering, Villigen, Switzerland, 2014.
[35] L. Xiao, J. Li, D.F. Brougham, E.K. Fox, N. Feliu, A. Bushmelev, et al., Water-soluble superparamagnetic magnetite nanoparticles with biocompatible coating for enhanced magnetic resonance imaging, ACS Nano 5 (2011) 6315–6324.
[36] C. Piquer, M.A. Laguna-Marco, A.G. Roca, R. Boada, C. Guglieri, J. Chaboy, Fe K-Edge X-ray absorption spectroscopy study of nanosized nominal magnetite, J. Phys. Chem. C 118 (2014) 1332–1346.
[37] M. Wilke, F. Farges, P.-E. Petit, G.E. Brown Jr, F. Martin, Oxidation state and coordination of Fe in minerals: an Fe K-XANES study, Am. Miner. 86 (2001) 714–730.
[38] M.E.F. Brollo, R. López-Ruiz, D. Muraca, S.J.A. Figueroa, K.R. Pirota, M. Knobel, Compact Ag@Fe_3O_4 core-shell nanoparticles by means of single-step thermal decomposition reaction, Sci. Rep. 4 (2014) 6839.
[39] M. Zhang, G. Pan, D. Zhao, G. He, XAFS study of starch-stabilized magnetite nanoparticles and surface speciation of arsenate, Environ. Pollut. 159 (2011) 3509–3514.
[40] O. Moscoso-Londoño, M.S. Carrião, C. Cosio-Castañeda, V. Bilovol, R. Martínez Sánchez, E.J. Lede, et al., One-step room temperature synthesis of very small γ-Fe_2O_3 nanoparticles, Mater. Res. Bull. 48 (2013) 3474–3478.
[41] G. Beaucage, Approximations leading to a unified exponential/power-law approach to small-angle scattering, J. Appl. Cryst. 28 (1995) 717–728.
[42] R. Hernández, J. Sacristán, A. Nogales, T.A. Ezquerra, C. Mijangos, Structural organization of iron oxide nanoparticles synthesized inside hybrid polymer gels derived from alginate studied with small-angle X-ray scattering, Langmuir 25 (2009) 13212–13218.
[43] M.B. Fernández van Raap, P. Mendoza Zélis, D.F. Coral, T.E. Torres, C. Marquina, G.F. Goya, et al., Self organization in oleic acid-coated $CoFe_2O_4$ colloids: a SAXS study, J. Nanopart. Res. 14 (2012) 1072.
[44] O. Glatter, O. Kratky, Small Angle X-ray Scattering, Academic Press, New York, 1982.
[45] J.M. Orozco-Henao, D.F. Coral, D. Muraca, O. Moscoso-Londoño, P. Mendoza Zélis, M.B. Fernandez van Raap, et al., Effects of nanostructure and dipolar interactions on magnetohyperthermia in iron oxide nanoparticles, J. Phys. Chem. C 120 (2016) 12796–12809.
[46] R. Hernández, J. Sacristán, A. Nogales, M. Fernández, T.A. Ezquerra, C. Mijangos, Structure and viscoelastic properties of hybrid ferrogels with iron oxide nanoparticles synthesized in situ, Soft Matter 6 (2010) 3910–3917.
[47] M.J. Park, J. Park, T. Hyeon, K. Char, Effect of interacting nanoparticles on the ordered morphology of block copolymer/nanoparticle mixtures, J. Polym. Sci. Pol. Phys. 44 (2006) 3571–3579.
[48] A. Tamion, C. Raufast, M. Hillenkamp, E. Bonet, J. Jouanguy, B. Canut, et al., Magnetic anisotropy of embedded Co nanoparticles: influence of the surrounding matrix, Phys. Rev. B 81 (2010) 144403.
[49] R. Aquino, J. Depeyrot, M.H. Sousa, F.A. Tourinho, E. Dubois, R. Perzynski, Magnetization temperature dependence and freezing of surface spins in magnetic fluids based on ferrite nanoparticles, Phys. Rev. B 72 (2005) 184435.
[50] C. Vazquez-Vazquez, M.A. Lopez-Quintela, M.C. Bujan-Nuñez, J. Rivas, Finite size and surface effects on the magnetic properties of cobalt ferrite nanoparticles, J. Nanopart. Res. 13 (2011) 1663–1676.
[51] T.N. Shendruk, R.D. Desautels, B.W. Southern, J. van Lierop, The effect of surface spin disorder on the magnetism of γ-Fe_2O_3 nanoparticle dispersions, Nanotechnology 18 (2007) 455704.
[52] M.P. Rowe, S. Sullivan, R.D. Desautels, E. Skoropata, J. van Lierop, Rational selection of superparamagnetic iron oxide/silica nanoparticles to create nano-composite inductors, J. Mater. Chem. C 3 (2015) 9789–9793.
[53] A. Demortière, P. Panissod, B.P. Pichon, G. Pourroy, D. Guillon, B. Donnio, et al., Size-dependent properties of magnetic iron oxide nanocrystals, Nanoscale 3 (2011) 225–232.
[54] F. Bloch, Zur Theorie des Ferromagnetismus, Z. Phys. 61 (1930) 206–219.
[55] M. Thakur, K. De, S. Giri, S. Si, A. Kotal, T.K. Mandal, Interparticle interaction and size effect in polymer coated magnetite nanoparticles, J. Phys. Condens. Mater. 18 (2006) 9093–9104.
[56] K. Parekh, R.V. Upadhyay, V.K. Aswal, Monodispersed superparamagnetic Fe_3O_4 nanoparticles: synthesis and characterization, J. Nanosci. Nanotechnol. 9 (2009) 2104–2110.
[57] S. Shekhar, E.P. Sajitha, V. Prasad, S.V. Subramanyam, High coercivity below percolation threshold in polymer nanocomposite, J. Appl. Phys. 104 (2008) 083910.
[58] C.-R. Lin, J.-S. Wang, T.-W. Sung, R.K. Chiang, Magnetic behavior of nanocomposites containing self-assembled magnetite particles dispersed in a paraffin wax matrix, IEEE Trans. Magn. 41 (2005) 3466–3468.
[59] K. Maaz, M. Usman, S. Karim, A. Mumtaz, S.K. Hasanain, M.F. Bertino, Magnetic response of core-shell cobalt ferrite nanoparticles at low temperature, J. Appl. Phys. 105 (2009) 113917.
[60] K. Maaz, A. Mumtaz, S.K. Hasanain, M.F. Bertino, Temperature dependent coercivity and magnetization of nickel ferrite nanoparticles, J. Magn. Magn. Mater. 322 (2010) 2199–2202.
[61] V.B. Barbeta, R.F. Jardim, K.P. Kiyohara, F.B. Effenberger, L.M. Rossi, Magnetic properties of Fe_3O_4 nanoparticles coated with oleic and dodecanoic acids, J. Appl. Phys. 107 (2010) 073913.
[62] P.V. Hendriksen, F. Bødker, S. Linderoth, S. Wells, S. Mørup, Ultrafine maghemite particles. I. Studies of induced magnetic texture, J. Phys. Condens. Mater. 6 (1994) 3081–3090.
[63] A. Franco Jr, V.S. Zapf, V.B. Barbeta, R.F. Jardim, Spin-wave fluctuations in ferrimagnetic $Mg_xFe_{3-x}O_4$ nanoparticles, J. Appl. Phys. 107 (2010) 073904.
[64] W.C. Nunes, W.S.D. Folly, J.P. Sinnecker, M.A. Novak, Temperature dependence of the coercive field in single-domain particle systems, Phys. Rev. B 70 (2004) 014419.
[65] T.E. Torres, E. Lima Jr, A. Mayoral, A. Ibarra, C. Marquina, M.R. Ibarra, et al., Validity of the Néel-Arrhenius model for highly anisotropic $Co_xFe_{3-x}O_4$ nanoparticles, J. Appl. Phys. 11 (2015) 183902.
[66] F.C. Fonseca, G.F. Goya, R.F. Jardim, R. Muccillo, N.L.V. Carreño, E. Longo, et al., Superparamagnetism and magnetic properties of Ni nanoparticles embedded in SiO_2, Phys. Rev. B 66 (2002) 104406.
[67] P.P. Vaishnava, R. Tackett, A. Dixit, C. Sudakar, R. Naik, G. Lawes, Magnetic relaxation and dissipative heating in ferrofluids, J. Appl. Phys. 102 (2007) 063914.
[68] C.P. Bean, J.D. Livingston, Superparamagnetism, J. Appl. Phys. 30 (1959) S120.
[69] K. Yosida, M. Tachiki, On the origin of the magnetic anisotropy energy of ferrites, Prog. Theor. Phys. 17 (1957) 331–359.
[70] G.F. Goya, T.S. Berquó, F.C. Fonseca, M.P. Morales, Static and dynamic magnetic properties of spherical magnetite nanoparticles, J. Appl. Phys. 94 (2003) 3520.
[71] A.D. Arelaro, A.L. Brandl, E. Lima Jr, L.F. Gamarra, G.E.S. Brito, W.M. Pontuschka, et al., Interparticle interactions and surface contribution to the effective anisotropy in biocompatible iron oxide nanoparticles used for contrast agents, J. Appl. Phys. 97 (2005) 10J316.
[72] F. Ludwig, E. Heim, M. Schilling, Characterization of superparamagnetic nanoparticles by analyzing the magnetization and relaxation dynamics using fluxgate magnetometers, J. Appl. Phys. 101 (2007) 113909.
[73] P. Allia, G. Barrera, P. Tiberto, T. Nardi, Y. Leterrier, M. Sangermano, Fe_3O_4 nanoparticles and nanocomposites with potential application in biomedicine and in communication technologies: nanoparticle aggregation, interaction, and effective magnetic anisotropy, J. Appl. Phys. 116 (2014) 113903.
[74] C. Sciancalepore, R. Rosa, G. Barrera, P. Tiberto, P. Allia, F. Bondioli, Microwave-assisted nonaqueous sol–gel synthesis of highly crystalline magnetite nanocrystals, Mater. Chem. Phys. 148 (2014) 117–124.
[75] M. Knobel, W.C. Nunes, A.L. Brandl, J.M. Vargas, L.M. Socolovsky, D. Zanchet, Interaction effects in magnetic granular systems, Physica B 354 (2004) 80–87.
[76] D. Kechrakos, K.N. Trohidou, Interplay of dipolar interactions and grain-size distribution in the giant magnetoresistance of granular metals, Phys. Rev. B 62 (2000) 3941.
[77] J.A. Mydosh, Spin Glasses, Taylor & Francis, Washington DC, 1993.
[78] S.H. Masunaga, R.F. Jardim, P.F.P. Fichtner, J. Rivas, Role of dipolar interactions in a system of Ni nanoparticles studied by magnetic susceptibility measurements, Phys. Rev. B 80 (2009) 184428.
[79] K. Nadeem, H. Krenn, T. Traussnig, R. Würschum, D.V. Szabó, I. Letofsky-Papst, Effect of dipolar and exchange interactions on magnetic blocking of maghemite nanoparticles, J. Magn. Magn. Mater. 323 (2011) 1998–2004.
[80] P. Poddar, T. Telem-Shafir, T. Fried, G. Markovich, Dipolar interactions in two- and three-dimensional magnetic nanoparticle arrays, Phys. Rev. B 66 (2002) 060403.
[81] M.F. Hansen, S. Morup, Estimation of blocking temperatures from ZFC/FC curves, J. Magn. Magn. Mater. 203 (1999) 214–216.
[82] J.C. Denardin, A.L. Brandl, M. Knobel, P. Panissod, A.B. Pakhomov, H. Liu, et al., Thermoremanence and zero-field-cooled/field-cooled magnetization study of $Co_x(SiO_2)_{1-x}$ granular films, Phys. Rev. B 65 (2002) 064422.

[83] G.M. Tsoi, U. Senaratne, R.J. Tackett, E.C. Buc, R. Naik, P.P. Vaishnava, et al., Memory effects and magnetic interactions in a γ-Fe_2O_3 nanoparticle system, J. Appl. Phys. 97 (2005) 10J507.
[84] M. Knobel, W.C. Nunes, H. Winnischofer, T.C.R. Rocha, L.M. Socolovsky, C.L. Mayorga, et al., Effects of magnetic interparticle coupling on the blocking temperature of ferromagnetic nanoparticle arrays, J. Non-Cryst. Solids 353 (2007) 743–747.
[85] F. Luis, F. Petroff, J.M. Torres, L.M. García, J. Bartolomé, J. Carrey, et al., Magnetic relaxation of interacting Co clusters: crossover from two- to three-dimensional lattices, Phys. Rev. Lett. 88 (2002) 217205.
[86] L.J. Bruvera, P. Mendoza Zélis, M. Pilar Calatayud, G.F. Goya, F.H. Sánchez, Determination of the blocking temperature of magnetic nanoparticles: the good, the bad, and the ugly, J. Appl. Phys. 118 (2015) 184304.
[87] B.D. Cullity, C.D. Graham, Introduction to Magnetic Materials, IEEE Press, Willey, Hoboken, New Jersey, 2009.
[88] M. El. Hilo, K. O´Grady, R.W. Chantrell, Interaction effects and activation volumes in barium ferrite recording media, IEEE Trans. Magn. 27 (1991) 4666–4668.
[89] M. Respaud, J.M. Broto, H. Rakoto, A.R. Fert, L. Thomas, B. Barbara, et al., Surface effects on the magnetic properties of ultrafine cobalt particles, Phys. Rev. B 57 (1998) 2925.
[90] J.S. Lee, R.P. Tan, J.H. Wu, Y.K. Kim, Effect of interparticle interactions and size dispersion in magnetic nanoparticle assemblies: a static and dynamic study, Appl. Phys. Lett. 99 (2011) 062506.
[91] W.C. Nunes, L.M. Socolovsky, J.C. Denardin, F. Cebollada, A.L. Brandl, M. Knobel, Role of magnetic interparticle coupling on the field dependence of the super-paramagnetic relaxation time, Phys. Rev. B 72 (2005) 212413.